Superconducting electronic state in optimally doped YBa$_2$Cu$_3$O$_{7-\delta}$ observed with laser-excited angle-resolved photoemission spectroscopy

M. Okawa,[1,*] K. Ishizaka,[1,2] H. Uchiyama,[3] H. Tadatomo,[4] T. Masui,[4] S. Tajima,[4] X.-Y. Wang,[5] C.-T. Chen,[5] S. Watanabe,[1]
A. Chainani,[6] T. Saitoh,[7] and S. Shin[1,2,6,†]

[1]*Institute for Solid State Physics, University of Tokyo, Kashiwa, Chiba 277-8581, Japan*
[2]*CREST, Japan Science and Technology Agency, Tokyo 102-0075, Japan*
[3]*Japan Synchrotron Radiation Research Institute, Sayo, Hyogo 679-5198, Japan*
[4]*Department of Physics, Osaka University, Toyonaka, Osaka 560-0043, Japan*
[5]*Technical Institute of Physics and Chemistry, Chinese Academy of Sciences, Beijing 100190, China*
[6]*RIKEN SPring-8 Center, Sayo, Hyogo 679-5148, Japan*
[7]*Department of Applied Physics, Tokyo University of Science, Tokyo 162-8601, Japan*

Low-energy electronic structure of optimally doped YBa$_2$Cu$_3$O$_{7-\delta}$ is investigated using laser-excited angle-resolved photoemission spectroscopy. The surface state and the CuO chain band that usually overlap the CuO$_2$ plane derived bands are not detected, thus enabling a clear observation of the bulk superconducting state. The observed bilayer splitting of the Fermi surface is ~0.08 Å^{-1} along $(0,0)-(\pi,\pi)$ direction, significantly larger than Bi$_2$Sr$_2$CaCu$_2$O$_{8+\delta}$. The kink structure of the band dispersion reflecting the renormalization effect at ~60 meV shows up similarly as in other hole-doped cuprates. The momentum dependence of the superconducting gap shows $d_{x^2-y^2}$-wave-like amplitude but exhibits a nonzero minimum of ~12 meV along the $(0,0)-(\pi,\pi)$ direction. Possible origins of such an unexpected "nodeless" gap behavior are discussed.

I. INTRODUCTION

The high-T_c superconductivity in cuprates is still attracting strong attention after extensive studies over 20 years. In particular, the concomitant technical progress of angle-resolved photoemission spectroscopy (ARPES) has significantly contributed to the investigation of high-T_c cuprates since its discovery, e.g., Fermi-surface determination and confirmation of the $d_{x^2-y^2}$-wave superconducting gap symmetry.[1] More recently, the "kink"-like structure in band dispersions was observed in a number of hole-doped cuprates, thus shedding light on the details of the electron-boson coupling and the renormalization effect.[1–6] Moreover, very recent arguments on the pseudogap and so-called the "Fermi arc" in relation to the mechanism of superconductivity have further enhanced the significance and effectiveness of ARPES studies on cuprates.[7–11] The ARPES results reported thus far, however, are mostly dominated by the data from a bismuth-based cuprate Bi$_2$Sr$_2$CaCu$_2$O$_{8+\delta}$ (BSCCO) and its related compounds because of the easiness of getting a clean surface by cleaving. For deeper understanding of the high-T_c superconductivity, systematic elucidation of the superconducting electronic structure across various compounds is still highly desired.

YBa$_2$Cu$_3$O$_{7-\delta}$ (YBCO) is one such typical cuprate system with relatively high T_c of 93 K, whose orthorhombic crystal structure is characterized by the existence of one-dimensional CuO chains besides bilayered CuO$_2$ planes.[12] Since samples of good quality are available in YBCO, the electric, magnetic, and phononic properties have been extensively studied by various kinds of probes, thus providing a number of important findings such as pseudo(spin)gap, magnetic-resonance mode, etc., at a very early stage.[13] Recently, owing to the progress of detwinning technique aligning the CuO chains perfectly in a single domain, in-plane anisotropic electronic properties are being revealed. Particularly, indication of the superconducting order parameter showing twofold $d_{x^2-y^2}+s$-wave symmetry has been concluded by many probes including optical,[14–16] phase sensitive,[17] and tunneling current[18] measurements. A precise investigation of the superconducting state in YBCO by high-resolution ARPES will be very valuable in order to give a comparative study across the various probes as well as compounds. A considerable amount of ARPES results have been reported so far.[19–25] However, a critical difficulty called the "surface state" is known to hinder the bulk electronic structure study of YBCO.[1,20,21] It had been long argued that this problem should arise from two kinds of the easy cleavage, CuO chain and BaO terminations, as observed by scanning tunneling microscope.[26,27] Recent effortful ARPES studies have successfully attributed the origin of the surface state to the first CuO$_2$ bilayer being excessively overdoped due to the termination.[23–25] Nakayama *et al.*[23] and Zabolotnyy *et al.*[24] also attained the partial observation of the bulk superconducting state beside the surface state but unfortunately not clearly around the momentum region where the superconducting gap takes the minimum (nodal region). To discuss the total low-energy electronic structure, more precise data without the influence of the surface state are necessary over a wide region of the Brillouin zone.

In this paper, we report the direct observation of the superconducting electronic state in optimally doped YBCO using laser-ARPES. By using a vacuum-ultraviolet (VUV) laser as the light source, the ARPES measurement with sub-meV resolution and bulk sensitivity is available.[28] We found clear band dispersions from the bulk state, showing the evolution of $d_{x^2-y^2}$-like superconducting gap. The surface state as well as the CuO chain band was not observed throughout

the momentum region of measurements, thus making the analysis of the superconducting CuO_2 band much easier. The observed bilayer splitting is larger than BSCCO but as expected by band calculations,[29,30] while the kink structure at ~ 60 meV appears similarly as in other hole-doped cuprates. The momentum dependence of the gap in detail takes a minimum of ~ 12 meV along $(0,0)-(\pi,\pi)$ direction, thus showing "nodeless" behavior. We discuss the possible origins of such an unusual superconducting state.

II. EXPERIMENTAL DETAILS

High-quality single crystals of optimally doped $YBa_2Cu_3O_{7-\delta}$ ($T_c = 93$ K) were grown by the crystal pulling method[31] and detwinned by annealing under uniaxial pressure. The sample orientation was determined by x-ray Laue diffraction and Raman-scattering measurements.

Photoemission experiments were performed by using a linearly polarized laser-ARPES system[28] equipped with a Scienta R4000 hemispherical electron analyzer and a quasicontinuous-wave VUV laser ($h\nu = 6.994$ eV) as a light source. Owing to its low kinetic energy, the escape depth of a photoelectron attains a value of ~ 100 Å,[32] thus enabling us a bulk sensitive measurement. The pressure was better than 5×10^{-11} Torr throughout the measurements. The spot size of the incident light was around ~ 200 μm. We obtained clean (001) surfaces of YBCO by cleaving *in situ* at 5–10 K. Sample degradation due to aging was not observed during the continuous measurement over 24 h. We set the total-energy resolution of the measurement system to 2–3 meV in order to gain in photoemission intensity. The Fermi level (E_F) was determined in accuracy of better than ± 0.5 meV by the Fermi edge of an evaporated Au film connected electrically to the sample. Unless specifically noted, the temperature of data acquisition is 5 K. For the transformation of angle to momentum, we used the value of 4.9 eV as the work function of YBCO.[33] For simplicity, we use "nodal direction" to represent the $\Gamma(0,0)$-$S(\pi,\pi)$ direction, following the custom of a normal $d_{x^2-y^2}$ superconductivity.

III. RESULTS AND DISCUSSIONS

A. Band dispersions and Fermi surface

Figures 1(a)–1(f) show the obtained ARPES intensity images as a function of binding energy (E_B) and momentum (k) along momentum cuts as indicated in Fig. 1(g). Here, we can observe clear band dispersions accompanying peaks near E_F. According to the band calculations for slightly overdoped YBCO ($\delta = 0$),[29,30] there are three Fermi surfaces expected; the bonding and antibonding two-dimensional Fermi surfaces arising from the bilayer coupling of CuO_2 planes and the one-dimensional surface from a CuO chain. These Fermi surfaces, whose k_z projections are shown by the shaded areas in Fig. 1(g), are expected to show large three dimensionality (k_z dependence) compared to BSCCO. The observed band dispersions in Figs. 1(a)–1(f) thus correspond to two-dimensional CuO_2 plane bands. With approaching Y point, the ARPES intensity becomes weak and the band dispersion becomes difficult to be distinguished from the background,
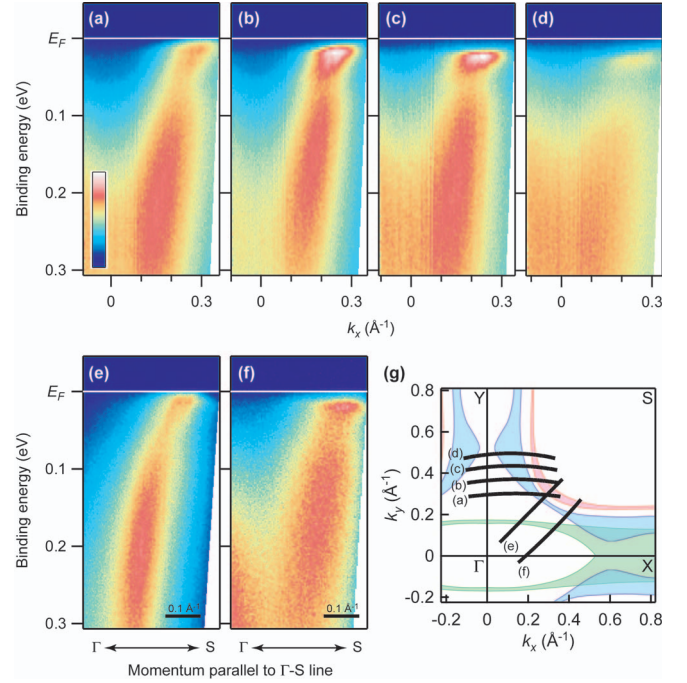

FIG. 1. (Color) [(a)–(f)] ARPES intensity images of optimally doped YBCO obtained at 5 K. (g) Schematic Fermi surfaces of YBCO in the first Brillouin zone. Red, blue, and green shaded areas indicate the k_z-projected Fermi surfaces of the bonding and antibonding CuO_2 bands and the CuO chain band, respectively, obtained from a band calculation (Ref. 29). The momentum cuts of the measurements for (a)–(f) are shown by black curves.

as shown in Fig. 1(d). This is possibly because of the transition matrix element effect in the photoemission process, concerning a significant $h\nu$ and k dependence in spectral weight.[23] On moving away from the nodal direction [(a, e) $\rightarrow$ (d, f) in Fig. 1], we can easily see that the top of the band dispersion tends to sink beneath E_F, indicative of a gap opening. This gapped feature clearly reveals the $d_{x^2-y^2}$-wave-like magnitude, i.e., the gap size $|\Delta|$ increases with approaching the antinodal (X or Y point) side. This ensures that the present observation of band dispersions indeed reflects the superconducting bulk CuO_2 electronic structure, possibly owing to the bulk sensitivity and/or the matrix element effect at $h\nu = 6.994$ eV. The details of the superconducting gap and the coherence peak shape will be discussed later (Sec. III B).

In addition to the superconducting gap, we can also recognize a clear band renormalization at ~ 60 meV, similarly as in other high-T_c cuprates. To elucidate the band renormalization character, band dispersions along several momentum cuts including the nodal direction are represented in Fig. 2(a).

These dispersions are obtained by plotting the peak positions of momentum distribution curves (MDCs), the momentum profiles of the ARPES intensity image at each energy. We estimated the peak position by fitting a Lorentzian curve to each MDC. We can easily find the band renormalization behavior in this dispersion at around 60 meV, both at nodal and off-nodal regions. The energy of this kink feature is quite similar to those reported previously in YBCO.[22,23] The kink also appears as the decrease in the peak width of MDCs
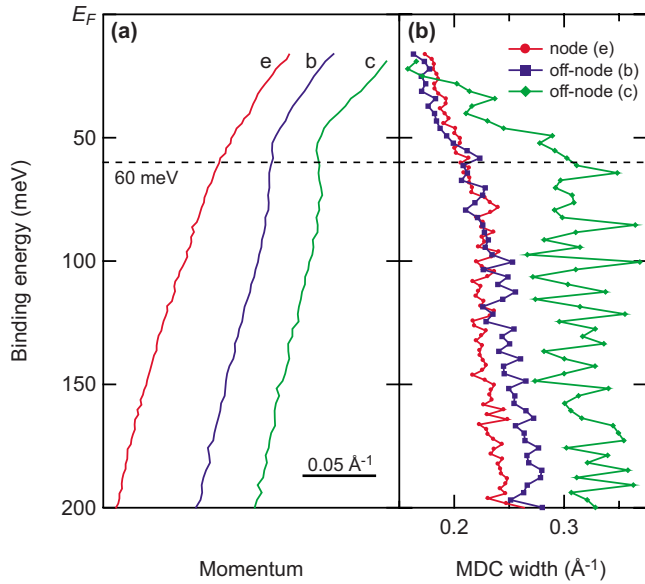
FIG. 2. (Color online) (a) Band dispersions obtained from MDC fittings at nodal and off-nodal regions. Labels (e), (b), and (c) correspond to the momentum cuts shown in Fig. 1(g). (b) Peak width of MDCs as a fuction of the binding energy.
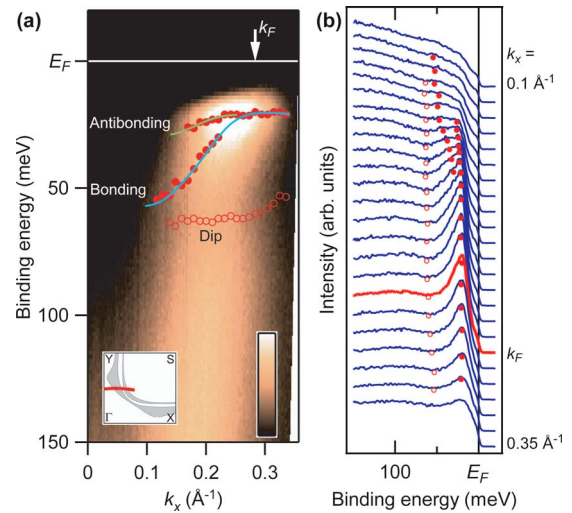

FIG. 3. (Color online) (a) ARPES intensity image and (b) EDCs at the off-nodal location as shown in the inset of (a). Closed circles denote the peak positions of EDCs, while the dip positions are represented by open circles. Curves are guides for eyes to show the bonding and antibonding band components. The k_F position of the outer bonding band is shown by an arrow.

below $\sim$60 meV, as shown in Fig. 2. The width of MDC peak is considered to be proportional to the imaginary part of the self-energy Im $\Sigma(\omega)$.[1] Thus, the above result indicates the suppression of the scattering rate below the kink energy. These data show stronger renormalization at the antinodal side than near the nodal direction, which is similar to the momentum dependence as observed in bismuth-based cuprates.[3,4] Thus we confirmed that the kink structure in hole-doped high-T_c cuprates shows a universal character also in the superconducting electronic state in YBCO.

Since the band calculations[29,30] predicted a large bilayer splitting of the CuO$_2$ bands, we look into the details of the band dispersions to see whether they are composed of two components, bonding and antibonding bands. Figures 3(a) and 3(b) show the band dispersion near E_F at the off-nodal region and its energy distribution curves (EDCs) which are the energy profiles of an ARPES intensity image.

At E_B<40 meV, which is sufficiently below the kink energy, the band dispersion shows fairly sharp peaks ($\sim$20 meV) with an indication of the superconducting gap opening as seen in the EDCs. To elucidate the fine details of the band structure, we plotted the peak positions of EDCs shown as closed circles in Fig. 3. Here, we found that there are two EDC peaks at around $k_x \sim 0.2$ Å^{-1}, indicating the existence of antibonding and bonding bands, as shown in Fig. 3(a). The Fermi wave vector (k_F) for the outer Fermi surface composed of bonding band can be determined as the k point where the peak position of the EDC most nearly approaches E_F, considering the manifestation of the superconducting Bogoliubov quasiparticle dispersion.[34] The k_F of the inner antibonding band, on the other hand, is very difficult to be precisely assigned since it merges with bonding band on approaching E_F. Note that the dip structure of EDCs indicated by open circles in Fig. 3 shows up at around 60 meV beside the quasiparticle peak, reflecting the band renor-

malization effect in the superconducting state. Regarding the renormalization energy at this off-nodal region, the above value is slightly lower compared to the 70 meV kink observed in BSCCO,[4] and similar that in YBCO reported by Nakayama *et al.*[23]

To separately estimate k_F for respective bands, we show the ARPES spectrum obtained along the Γ-S direction in Fig. 4(a). Its MDCs are also shown in Fig. 4(b).

We can see that each MDC contains two broad peaks. Each MDC was well fitted by a sum of two Lorentzians with a constant background $I(k)=\Sigma_{i=1}^{2}(A_i/\pi)(\Gamma_i/[(k-k_i)^2+\Gamma_i^2])+C$ at the energy region of E_B<50 meV, as shown in Fig. 4(b). The peak positions obtained by the MDC fitting (k_1 and k_2) as observed in Fig. 4(a) suggest the bilayer splitting of about $\Delta k = 0.08$ Å^{-1}, which agrees well with band
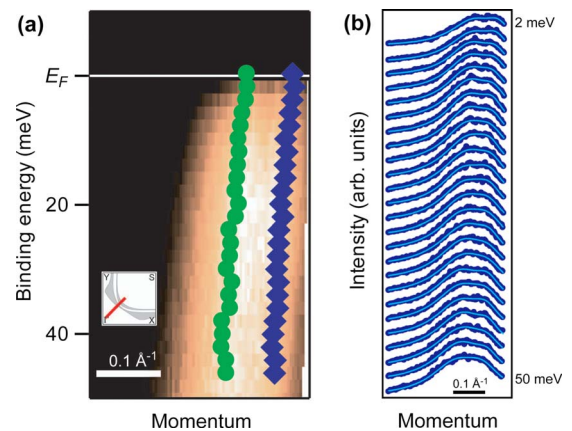

FIG. 4. (Color online) (a) ARPES intensity image and (b) MDCs along the cut near the Γ-S direction as shown in the inset. Circles and squares denote peak positions of the two Lorentzians obtained by fitting MDCs as shown in (b), respectively, indicating antibonding and bonding band.
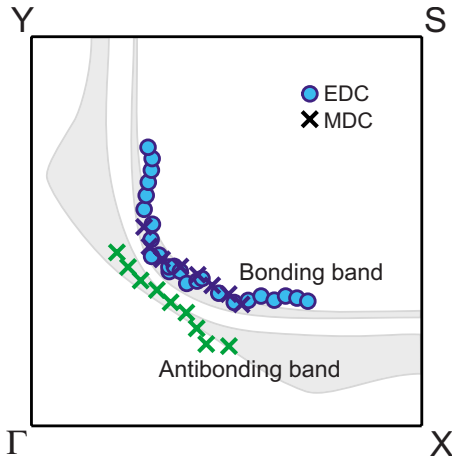
FIG. 5. (Color online) k_F positions plotted on the Brillouin zone. Circles shows k_F determined as the position where EDC peak most nearly approaches E_F (see Fig. 3). Crosses represent the MDC peak positions near E_F (see Fig. 4).

calculations.[29,30] The values of the half width at half maximum for respective peaks (Γ_1 and Γ_2), on the other hand, are about 0.1 and 0.2 Å^{-1} for bonding and antibonding bands at near E_F, which are considerably broader than those in BSCCO (e.g., 0.0031 Å^{-1} for an optimally doped sample in Ref. 35). This broadening makes it difficult to clearly distinguish the bilayer splitting in YBCO despite its large value compared to BSCCO (shown later). It may be partly due to the greater k_z dispersion expected in YBCO, giving rise to broadening effect.[36–38] To more clearly separate the bilayer split dispersion, investigations of more heavily doped samples may be useful as reported in BSCCO system, which remains to be elucidated in future.

By plotting k_F positions on the Brillouin zone, we can obtain the Fermi surface as shown in Fig. 5. Circles indicate the k_F which were obtained by tracing the EDC peak positions as previously described, while the cross markers represent the MDC peak positions at E_F. We could not observe any spectra corresponding to the CuO chain band as shown in Figs. 1(e) and 1(f), which may be due to the matrix element effect.[39] Apparently, k_F obtained from EDC is in a good correspondence with the outer bonding band Fermi surface we derived from MDC peaks. Here, we can confirm that the bilayer splitting occurs in a wide momentum region in YBCO, including the $(0,0)-(\pi,\pi)$ direction, where in BSCCO a very small splitting ($\Delta k = 0.014 - 0.015$ Å^{-1} in Ref. 40 and $\Delta k = 0.0075$ Å^{-1} in Ref. 41) is observed. Both of the bonding and antibonding band Fermi surfaces agree quite well with the local-density approximation (LDA) band calculation[29,30] and a previous report of the nodal bilayer splitting in YBCO.[22] A past ARPES study reporting the bulk electronic state of YBCO using 46 eV photon,[23] nevertheless, exhibited very small bilayer splitting of $\Delta k \sim 0.02 - 0.03$ Å^{-1} at the off-nodal region while our data show $\Delta k \sim 0.09$ Å^{-1} at a similar momentum region. This difference indicates that the bulk electronic state of YBCO may have significant three dimensionality compared to BSCCO, thus causing a strong $h\nu$ dependence in ARPES result.[42]
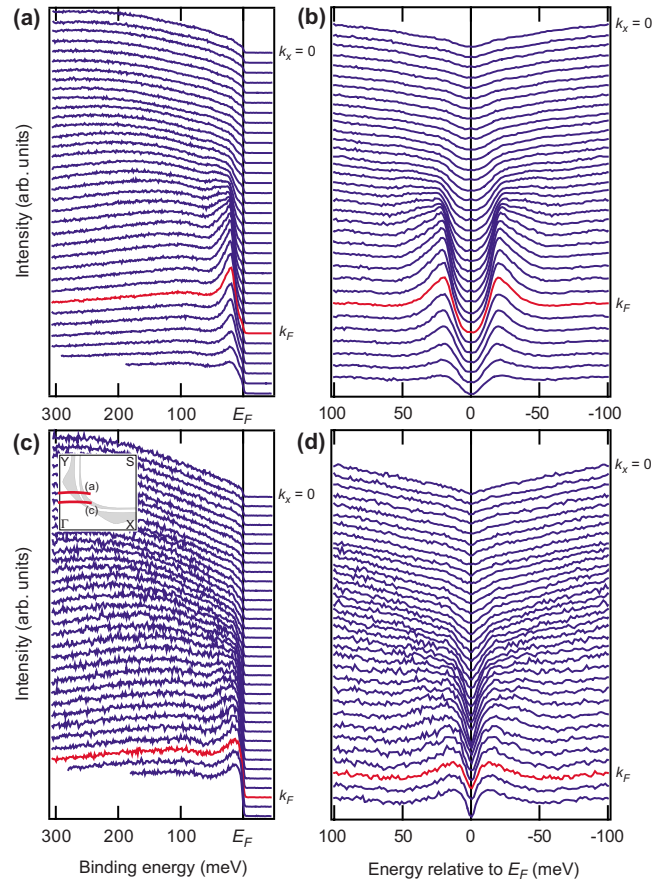

FIG. 6. (Color online) [(a) and (c)] EDCs along the momentum cutoff and on the nodal point. The inset in (c) shows each momentum cut of the measurements. [(b) and (d)] EDCs from (a) and (c) symmetrized at E_F.

B. Superconducting gap anisotropy

Here we focus on the evaluation of the superconducting gap and its anisotropy. In order to estimate the gap magnitude carefully, we show EDCs along the off-nodal direction and those symmetrized at E_F in Figs. 6(a) and 6(b), respectively. The symmetrized EDC spectrum can be expressed by $I_{sym}(\omega) = I(-\omega) + I(\omega)$, where $I(\omega)$ is the intensity of EDC as a function of ω and energy relative to E_F. As we described in Sec. III A, k_F of the outer bonding band can be determined as the k position where EDC peak most nearly approaches E_F, i.e., the peaks forming a pair in $I_{sym}(\omega)$ get closest to each other. In Fig. 7(a), we show the closeup of the EDCs at k_F and $k_x = 0$ extracted from Fig. 6(a). The EDC at k_F clearly indicates a sharp peak at ~ 20 meV and reduced intensity around E_F. Such spectral features represent the opening of the superconducting gap and the evolution of the Bogoliubov quasiparticle peak. The small edgelike component at E_F partly arises from the (angle-integrated type) background, as also observed at $k_x = 0$ where no band dispersion exists near E_F. The remaining may be due to the tail-like states of the coherence peak with finite lifetime, while we cannot completely rule out the subtle inclusion of the surface state. Nevertheless, the dominant spectral shape is very close to what is observed in BSCCO, indicating that the superconducting gap
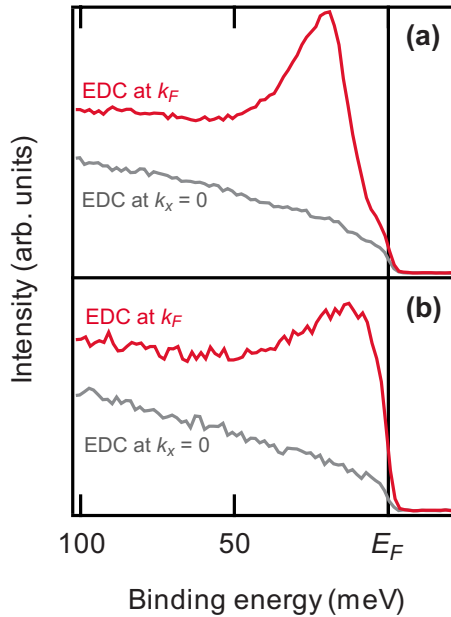
FIG. 7. (Color online) [(a) and (b)] Comparison of EDC at k_F to that at $k_x = 0$ along off- and on-nodal momentum cuts, extracted from the data in Figs. 6(a) and 6(c), respectively.

can be precisely investigated similarly in YBCO.

To discuss the momentum dependence of the superconducting gap, we show in Figs. 8(a)–8(c) EDCs at k_F and those symmetrized at E_F, for respective positions along the Fermi-surface contour as shown in Fig. 8(d). We can see a

systematic behavior that the gap size increases on approaching the antinodal X and Y points, in accord with a $d_{x^2-y^2}$-wave-like gap symmetry. A surprising result appears near the nodal point, nevertheless, as the persistent existence of a small gap on crossing the Γ-S line. Even at the momentum point along Γ-S direction where the gap size becomes minimum [corresponds to (1) and (i) in Fig. 8(b) and $\phi \approx 45°$ in Fig. 8(c)], the spectrum clearly shows a gapped feature thus indicating the nodeless character of the superconducting gap. Near the antinodal X and Y regions, the EDC shows a fairly weak coherence peak with high background level, reflecting the loss of ARPES intensity due to the matrix element effect. On approaching the Γ-S direction, on the other hand, the coherence peak intensity evolves and gets sharp in width, as is also observed in BSCCO. In the very vicinity of the Γ-S line, however, the coherence peak seems to become suppressed and broadened even though the higher energy part ($\gtrsim 0.1$ eV) of the dispersion remains clearly [Figs. 1(a) and 1(e)]. Such behavior is fairly unusual among hole-doped high-T_c cuprates, where the nodal quasiparticle tends to show a robust coherence.

To show the validity of our data analysis, we plot the raw EDCs along the cut where the gap minimum appears in Fig. 6(c). Comparing to the off-nodal point as shown in Fig. 6(a), the band dispersion approaches somewhat closer to E_F. The EDCs and those symmetrized [Fig. 6(d)], however, persistently show a clear gap across k_F. In Fig. 7(b), we show the EDC spectrum at k_F together with that at $k_x = 0$. We can clearly see a peak structure at ~12 meV for EDC at k_F, which is responsible for the gap feature. By comparing these
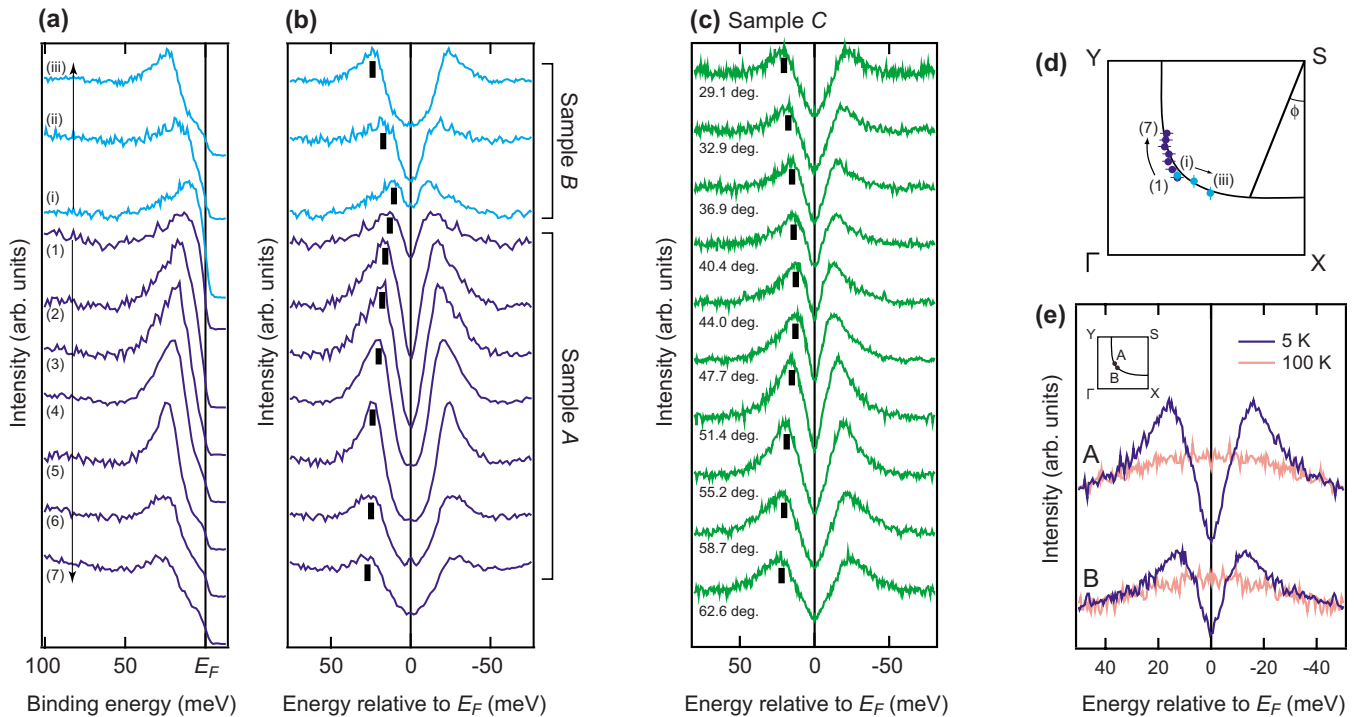

FIG. 8. (Color online) (a) EDCs at k_F and (b) those symmetrized at E_F obtained at momentum positions (1)–(7) and (i)–(iii) as indicated in (d). (1)–(7) and (i)–(iii) are the results from two different samples (samples A and B) along momentum cuts parallel to the Γ-X and Γ-Y directions, respectively. (c) Symmetrized EDCs at k_F obtained from one sample (sample C) along momentum cuts parallel to the Γ-S direction. Each k_F position is represented by the Fermi-surface angle ϕ as indicated in (d). (e) Symmetrized EDCs at the temperature of 5 and 100 K. A and B correspond to spectra at off-nodal and nodal points as shown in the inset.
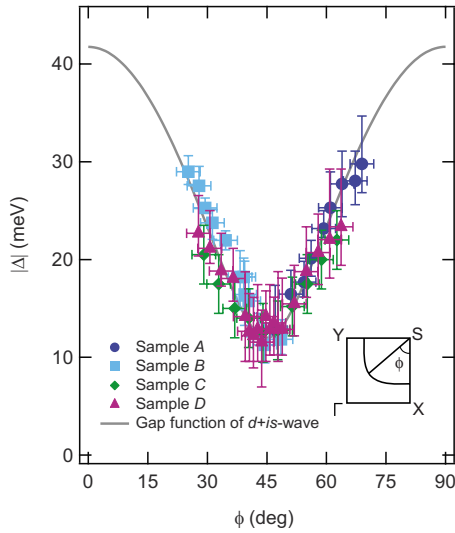
FIG. 9. (Color online) The gap size $|\Delta|$ plotted as a function of the Fermi-surface angle ϕ obtained from four different samples A–D. Here, the samples A–C are identical to those shown in Figs. 8(a)–8(c). The curve is the gap function of $d_{x^2-y^2}+is$ wave, where $\Delta_d=40$ meV and $\Delta_s=10$ meV. The error bars arise from the experimental uncertainty of the EDC peak positions and the estimation of the momentum value.

two spectra at k_F and $k_x=0$, we can rule out the possibility that this gap structure is due to the background (angle-integrated) component. In addition, we show the temperature dependence of the symmetrized EDC at k_F for (A) off-nodal and (B) nodal points in Fig. 8(e). Both of them clearly show the gap structure disappearing between 5 and 100 K ($>T_c$ $=93$ K). This indicates that this "nodal gap" evolution also reflects some modification of the electronic state, such as superconducting transition.

Now we discuss the gap symmetry by plotting $|\Delta|$ as a function of the Fermi-surface angle, ϕ (Fig. 9). We estimated the gap magnitudes by taking the energy position of the coherence peaks in the symmetrized EDCs at k_F. In order to confirm the reproducibility, we obtained ARPES data from seven different samples and found that all of their results coincide within errors. Four of them are shown here (samples A–D). Our result indicates that the momentum dependence of the gap in the observed region is nearly symmetric with respect to $\phi=45°$, where the gap shows the minimum of ~ 12 meV. Note that the nodes should shift to $\phi=45°+\delta\phi$ (e.g., $\delta\phi\sim-3°$ from Ref. 17) in case of $d_{x^2-y^2}+s$ wave but do not disappear unless the s-wave component dominates that of $d_{x^2-y^2}$ wave. A clear difference of the gap size between X and Y regions (e.g., the X-Y anisotropy ratio of the gap magnitude Δ_Y/Δ_X is larger than ~ 1.22 in Ref. 18), indicative of the $d_{x^2-y^2}+s$-wave-like anisotropy, is also not observed. Precise measurements covering the whole Brillouin zone (both X and Y points) are further necessary, nevertheless, to make any definite conclusion on the X-Y anisotropy of the gap.[39] Assuming that the observed gap character arises from a single superconducting state, a time-reversal symmetry broken state such as $d_{x^2-y^2}+is$ or $d_{x^2-y^2}+id_{xy}$ wave must be taken into account in order to reproduce such a nodeless $d_{x^2-y^2}$-wave-like symmetry.[43,44] Here we tentatively tried fit-
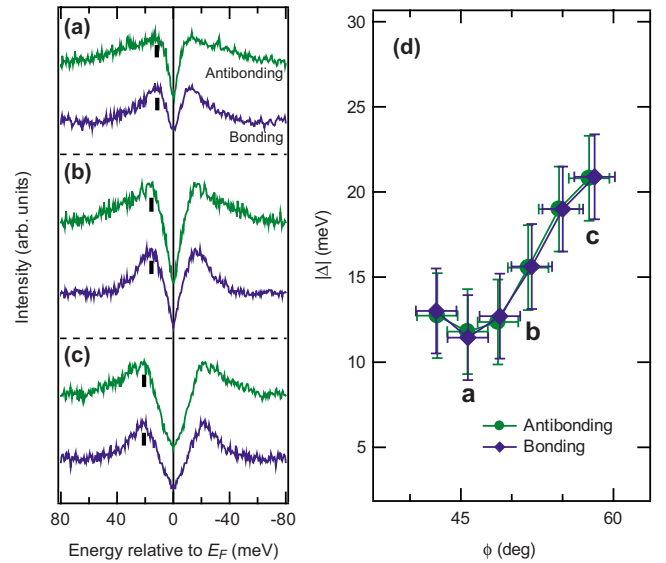

FIG. 10. (Color online) [(a)–(c)] Symmetrized EDCs at k_F along antibonding and the bonding band Fermi sheets. Estimated gaps for respective bands are shown in (d) as a function of ϕ.

ting the ϕ dependence with the $d_{x^2-y^2}+is$ symmetry gap function $\Delta_{d+is}=\Delta_d\cos(2\phi)+i\Delta_s$ as shown in Fig. 9, and obtained $\Delta_d=40$ meV and $\Delta_s=10$ meV.

The Fermi-surface dependences of the superconducting gap magnitude and its anisotropy should be also considered, which are actually observed in several multiband superconductors such as $2H$-NbSe$_2$,[45,46] MgB$_2$,[47,48] and a novel FeAs-based high-T_c superconductor.[49] In Fig. 10, we show the ϕ dependence of $|\Delta|$ for the two bilayer-split bonding and antibonding bands. The symmetrized EDCs at k_F are shown along respective Fermi sheets, where each k_F was estimated from the MDC fitting as shown in Fig. 4. ϕ dependence of $|\Delta|$ for bonding and antibonding bands are similar to each other, both showing the gap minimum of $|\Delta|\sim12$ meV at around $\phi=45°$ as discussed above. From this result, we cannot find any significant Fermi sheet dependence of $|\Delta|$ at least in this momentum region of measurement.

Now let us discuss the possible origins of the nodeless behavior of the superconducting gap. This result is in a strong contrast to many recent macroscopic experimental reports on YBCO.[15–18] Such behavior has not been either observed by ARPES in other cuprate superconductors until now. To explain this unusual data, here we discuss its possible origins, mainly in comparison with BSCCO. The first possibility we must suggest is the possible effect of the surface roughness in YBCO arising from two types of the surface terminations (CuO chain and BaO layers) obtained upon cleaving.[26,27] If there is a serious microscopic roughness at the surface, it may disturb the conservation law of the photoelectron momentum as the boundary condition. Thus the nodal gap might be reflecting the average gap value around the nodal point in the momentum space. If this is the case, the spectrum at off-nodal region should show a broader peak feature than that at node, because of the greater gap distribution as a function of ϕ. The EDC spectrum at off-nodal point, nevertheless, actually shows a much sharper feature as

shown in Fig. 7, which does not agree well with the above scenario. Another major difference between YBCO and BSCCO is the existence of the CuO chain structure along b axis, which may cause D_{2h} symmetrylike modification of the gap as represented by the $d_{x^2-y^2}+s$ wave. It is unlikely to be the origin of $d_{x^2-y^2}+is$-like superconducting gap as we observed, however, which holds D_{4h} symmetry. The remaining factors we should consider are the higher out-of-plane electron hopping and the greater bilayer coupling compared to BSCCO and related materials, which generate two well separated bonding and antibonding Fermi sheets with relatively high three-dimensional dispersions. Note that the ratio of out-of-plane and in-plane resistivity is $\rho_c/\rho_{ab} \sim 10^2$ in YBCO, while $\rho_c/\rho_{ab} \sim 10^5$ in BSCCO.[50] Such three-dimensional electronic structure, which is not usually taken into account, may be playing a relevant role. For example, some unexpected electronic state at the (001) surface may show up, as the time-reversal symmetry broken superconducting state discussed in the (110) surface of a $d_{x^2-y^2}$-wave superconductor.[51,52] In addition, the strong three-dimensional dispersion can induce the electron pairing along the k_z direction. A muon spin rotation (μSR) study[53] actually revealed the possible existence of an s-wave superconducting component along c axis. Theoretical consideration how a k_z-dependent superconducting component can be detected by various kinds of probes, including ARPES, is needed. Finally, we refer to several interesting reports regarding the pseudogap behavior in under and optimally doped YBCO.[54,55] These studies insist that a hidden order phase, such as charge/spin-density waves[56] or time-reversal symmetry broken staggered current flux states,[57,58] coexists with the superconducting phase below the pseudogap temperature ($T^* = 40 - 60$ K in optimally doped YBCO). This pseudogap phase may be associated with the nodal gap evolution. The origins cannot yet be clarified at present, nevertheless, it shows a possibility of a novel unconventional superconducting state realizing in YBCO. Further precise experimental and theoretical studies for its microscopic description are highly desired.

IV. CONCLUSIONS

We have investigated the low-energy electronic structure of optimally doped YBCO by using VUV laser ARPES. The unwanted surface state as well as CuO chain band were not detected perhaps because of the bulk sensitivity or the matrix element effect at $h\nu = 6.994$ eV. Thus we succeeded in the clear observation of the superconducting state in YBCO, which had been long desired. As a universal feature for high-T_c cuprates, the band renormalization effect caused by the electron-boson coupling was found at ~60 meV. The wide bilayer splitting of the Fermi surface was also confirmed for the superconducting electronic state, in good accordance with band calculations. Regarding the momentum dependence of the superconducting gap, we found the $d_{x^2-y^2}$-like behavior but without a clear evidence of gap node, showing the gap minimum of ~12 meV along Γ-S direction. This gap feature was similarly observed for both of the bilayer-split Fermi surfaces. This nodeless character of the gap raises the possibility of an unusual superconducting state appearing in YBCO, thus motivating further systematic studies.

ACKNOWLEDGMENTS

*m-okawa@issp.u-tokyo.ac.jp

†shin@issp.u-tokyo.ac.jp

[1] A. Damascelli, Z. Hussain, and Z.-X. Shen, Rev. Mod. Phys. **75**, 473 (2003).

[2] A. Lanzara, P. V. Bogdanov, X. J. Zhou, S. A. Kellar, D. L. Feng, E. D. Lu, T. Yoshida, H. Eisaki, A. Fujimori, K. Kishio, J.-I. Shimoyama, T. Noda, S. Uchida, Z. Hussain, and Z.-X. Shen, Nature (London) **412**, 510 (2001).

[3] T. Sato, H. Matsui, T. Takahashi, H. Ding, H.-B. Yang, S.-C. Wang, T. Fujii, T. Watanabe, A. Matsuda, T. Terashima, and K. Kadowaki, Phys. Rev. Lett. **91**, 157003 (2003).

[4] T. Cuk, F. Baumberger, D. H. Lu, N. Ingle, X. J. Zhou, H. Eisaki, N. Kaneko, Z. Hussain, T. P. Devereaux, N. Nagaosa, and Z.-X. Shen, Phys. Rev. Lett. **93**, 117003 (2004).

[5] T. Sato, K. Terashima, K. Nakayama, H. Matsui, T. Takahashi, K. Kadowaki, M. Kofu, and K. Hirota, J. Phys. Soc. Jpn. **76**, 103707 (2007).

[6] J. Wei, Y. Zhang, H. W. Ou, B. P. Xie, D. W. Shen, J. F. Zhao, L. X. Yang, M. Arita, K. Shimada, H. Namatame, M. Taniguchi, Y. Yoshida, H. Eisaki, and D. L. Feng, Phys. Rev. Lett. **101**, 097005 (2008).

[7] K. Tanaka, W. S. Lee, D. H. Lu, A. Fujimori, T. Fujii, Risdiana, I. Terasaki, D. J. Scalapino, T. P. Devereaux, Z. Hussain, and Z.-X. Shen, Science **314**, 1910 (2006).

[8] T. Kondo, T. Takeuchi, A. Kaminski, S. Tsuda, and S. Shin, Phys. Rev. Lett. **98**, 267004 (2007).

[9] W. S. Lee, I. M. Vishik, K. Tanaka, D. H. Lu, T. Sasagawa, N. Nagaosa, T. P. Devereaux, Z. Hussain, and Z.-X. Shen, Nature (London) **450**, 81 (2007).

[10] A. Kanigel, M. R. Norman, M. Randeria, U. Chatterjee, S. Souma, A. Kaminski, H. M. Fretwell, S. Rosenkranz, M. Shi, T. Sato, T. Takahashi, Z. Z. Li, H. Raffy, K. Kadowaki, D. Hinks, L. Ozyuzer, and J. C. Campuzano, Nat. Phys. **2**, 447 (2006).

[11] A. Kanigel, U. Chatterjee, M. Randeria, M. R. Norman, S. Souma, M. Shi, Z. Z. Li, H. Raffy, and J. C. Campuzano, Phys. Rev. Lett. **99**, 157001 (2007).

[12] J. D. Jorgensen, M. A. Beno, D. G. Hinks, L. Soderholm, K. J. Volin, R. L. Hitterman, J. D. Grace, I. K. Schuller, C. U. Segre, K. Zhang, and M. S. Kleefisch, Phys. Rev. B **36**, 3608 (1987).

[13] T. Timusk and B. Statt, Rep. Prog. Phys. **62**, 61 (1999).

[14] D. N. Basov, R. Liang, D. A. Bonn, W. N. Hardy, B. Dabrowski, M. Quijada, D. B. Tanner, J. P. Rice, D. M. Ginsberg, and T. Timusk, Phys. Rev. Lett. **74**, 598 (1995).

[15] M. F. Limonov, A. I. Rykov, S. Tajima, and A. Yamanaka, Phys. Rev. Lett. **80**, 825 (1998); Phys. Rev. B **61**, 12412 (2000).

[16] R. Nemetschek, R. Hackl, M. Opel, R. Philipp, M. T. Béal-Monod, J. B. Bieri, K. Maki, A. Erb, and E. Walker, Eur. Phys. J. B **5**, 495 (1998).

[17] J. R. Kirtley, C. C. Tsuei, Ariando, C. J. M. Verwijs, S. Harkema, and H. Hilgenkamp, Nat. Phys. **2**, 190 (2006).

[18] H. J. H. Smilde, A. A. Golubov, Ariando, G. Rijnders, J. M. Dekkers, S. Harkema, D. H. A. Blank, H. Rogalla, and H. Hilgenkamp, Phys. Rev. Lett. **95**, 257001 (2005).

[19] B. W. Veal and C. Gu, J. Electron Spectrosc. Relat. Phenom. **66**, 321 (1994).

[20] M. C. Schabel, C. H. Park, A. Matsuura, Z. X. Shen, D. A. Bonn, X. Liang, and W. N. Hardy, Phys. Rev. B **57**, 6090 (1998); **57**, 6107 (1998).

[21] D. H. Lu, D. L. Feng, N. P. Armitage, K. M. Shen, A. Damascelli, C. Kim, F. Ronning, Z.-X. Shen, D. A. Bonn, R. Liang, W. N. Hardy, A. I. Rykov, and S. Tajima, Phys. Rev. Lett. **86**, 4370 (2001).

[22] S. V. Borisenko, A. A. Kordyuk, V. Zabolotnyy, J. Geck, D. Inosov, A. Koitzsch, J. Fink, M. Knupfer, B. Büchner, V. Hinkov, C. T. Lin, B. Keimer, T. Wolf, S. G. Chiuzbăian, L. Patthey, and R. Follath, Phys. Rev. Lett. **96**, 117004 (2006).

[23] K. Nakayama, T. Sato, K. Terashima, H. Matsui, T. Takahashi, M. Kubota, K. Ono, T. Nishizaki, Y. Takahashi, and N. Kobayashi, Phys. Rev. B **75**, 014513 (2007).

[24] V. B. Zabolotnyy, S. V. Borisenko, A. A. Kordyuk, J. Geck, D. S. Inosov, A. Koitzsch, J. Fink, M. Knupfer, B. Büchner, S.-L. Drechsler, H. Berger, A. Erb, M. Lambacher, L. Patthey, V. Hinkov, and B. Keimer, Phys. Rev. B **76**, 064519 (2007).

[25] M. A. Hossain, J. D. F. Mottershead, D. Fournier, A. Bostwick, J. L. McChesney, E. Rotenberg, R. Liang, W. N. Hardy, G. A. Sawatzky, I. S. Elfimov, D. A. Bonn, and A. Damascelli, Nat. Phys. **4**, 527 (2008).

[26] H. L. Edwards, J. T. Markert, and A. L. de Lozanne, Phys. Rev. Lett. **69**, 2967 (1992).

[27] M. Maki, T. Nishizaki, K. Shibata, and N. Kobayashi, J. Phys. Soc. Jpn. **70**, 1877 (2001).

[28] T. Kiss, T. Shimojima, K. Ishizaka, A. Chainani, T. Togashi, T. Kanai, X.-Y. Wang, C.-T. Chen, S. Watanabe, and S. Shin, Rev. Sci. Instrum. **79**, 023106 (2008).

[29] O. K. Andersen, A. I. Liechtenstein, O. Jepsen, and F. Paulsen, J. Phys. Chem. Solids **56**, 1573 (1995).

[30] O. K. Andersen, O. Jepsen, A. I. Liechtenstein, and I. I. Mazin, Phys. Rev. B **49**, 4145 (1994).

[31] Y. Yamada and Y. Shiohara, Physica C **217**, 182 (1993).

[32] M. P. Seah and W. A. Dench, Surf. Interface Anal. **1**, 2 (1979).

[33] G. Rietveld, N. Y. Chen, and D. van der Marel, Phys. Rev. Lett. **69**, 2578 (1992).

[34] M. R. Norman, H. Ding, M. Randeria, J. C. Campuzano, T. Yokoya, T. Takeuchi, T. Takahashi, T. Mochiku, K. Kadowaki, P. Guptasarma, and D. G. Hinks, Nature (London) **392**, 157 (1998).

[35] K. Ishizaka, T. Kiss, S. Izumi, M. Okawa, T. Shimojima, A. Chainani, T. Togashi, S. Watanabe, C.-T. Chen, X. Y. Wang, T. Mochiku, T. Nakane, K. Hirata, and S. Shin, Phys. Rev. B **77**, 064522 (2008).

[36] A. Bansil, M. Lindroos, S. Sahrakorpi, and R. S. Markiewicz, Phys. Rev. B **71**, 012503 (2005).

[37] R. S. Markiewicz, S. Sahrakorpi, M. Lindroos, H. Lin, and A. Bansil, Phys. Rev. B **72**, 054519 (2005).

[38] S. Sahrakorpi, M. Lindroos, R. S. Markiewicz, and A. Bansil, Phys. Rev. Lett. **95**, 157601 (2005).

[39] In all the samples which we succeeded in observing the superconducting dispersion, CuO chain band was not detected. In the low-energy photoemission process using 6.994 eV light, the final state is considered to be a rather bandlike character, unlike the free-electron picture assumed to be held in conventional high-energy photoemission spectroscopy. This will make the matrix element effect strongly dependent on the incident light energy in relation to the final state and make it difficult to quantitatively simulate its effect. The $h\nu$-dependent ARPES using a low-energy synchrotron light will be useful to obtain more information concerning the matrix element effect in YBCO.

[40] A. A. Kordyuk, S. V. Borisenko, A. N. Yaresko, S.-L. Drechsler, H. Rosner, T. K. Kim, A. Koitzsch, K. A. Nenkov, M. Knupfer, J. Fink, R. Follath, H. Berger, B. Keimer, S. Ono, and Y. Ando, Phys. Rev. B **70**, 214525 (2004).

[41] T. Yamasaki, K. Yamazaki, A. Ino, M. Arita, H. Namatame, M. Taniguchi, A. Fujimori, Z.-X. Shen, M. Ishikado, and S. Uchida, Phys. Rev. B **75**, 140513(R) (2007).

[42] The in-plane and out-of-plane momenta ($k_{\parallel}$ and k_z) at fixed emission angle θ are given by $k_{\parallel} = \sqrt{\frac{2m}{\hbar^2}(h\nu + W - E_B)}\sin\theta$, $k_z = \sqrt{\frac{2m}{\hbar^2}[(h\nu + W - E_B)\cos^2\theta + V_0]}$, where m is the electron mass, W is the work function, and V_0 is the inner potential. k_z varies periodically as a function of $h\nu$, while its absolute value is difficult to be confirmed since V_0 is unknown. Regarding $k_{\parallel}$, the region of measurement is limited by $|k_{\parallel}| < 0.74$ Å^{-1} in the present setup with $h\nu = 6.994$ eV. For details, see, e.g., S. Hüfner, *Photoelectron Spectroscopy: Principles and Applications*, 3rd ed. (Springer, Berlin, 2003).

[43] D. J. Van Harlingen, Rev. Mod. Phys. **67**, 515 (1995).

[44] C. C. Tsuei and J. R. Kirtley, Rev. Mod. Phys. **72**, 969 (2000).

[45] T. Yokoya, T. Kiss, A. Chainani, S. Shin, M. Nohara, and H. Takagi, Science **294**, 2518 (2001).

[46] T. Kiss, T. Yokoya, A. Chainani, S. Shin, T. Hanaguri, M. Nohara, and H. Takagi, Nat. Phys. **3**, 720 (2007).

[47] S. Souma, Y. Machida, T. Sato, T. Takahashi, H. Matsui, S.-C. Wang, H. Ding, A. Kaminski, J. C. Campuzano, S. Sasaki, and K. Kadowaki, Nature (London) **423**, 65 (2003).

[48] S. Tsuda, T. Yokoya, Y. Takano, H. Kito, A. Matsushita, F. Yin, J. Itoh, H. Harima, and S. Shin, Phys. Rev. Lett. **91**, 127001 (2003).

[49] H. Ding, P. Richard, K. Nakayama, K. Sugawara, T. Arakane, Y. Sekiba, A. Takayama, S. Souma, T. Sato, T. Takahashi, Z. Wang, X. Dai, Z. Fang, G. F. Chen, J. L. Luo, and N. L. Wang, EPL **83**, 47001 (2008).

[50] H. R. Ott, in *The Physics of Superconductors*, Conventional and High-T_c Superconductors Vol. I, edited by K. H. Bennemann and J. B. Ketterson (Springer, Berlin, 2003), pp. 385–494.

[51] M. Matsumoto and H. Shiba, J. Phys. Soc. Jpn. **64**, 3384 (1995); **64**, 4867 (1995); **65**, 2194 (1996).

[52] M. Covington, M. Aprili, E. Paraoanu, L. H. Greene, F. Xu, J. Zhu, and C. A. Mirkin, Phys. Rev. Lett. **79**, 277 (1997).

[53] R. Khasanov, S. Strässle, D. Di Castro, T. Masui, S. Miyasaka, S. Tajima, A. Bussmann-Holder, and H. Keller, Phys. Rev. Lett. **99**, 237601 (2007).

[54] J. E. Sonier, J. H. Brewer, R. F. Kiefl, R. I. Miller, G. D. Morris, C. E. Stronach, J. S. Gardner, S. R. Dunsiger, D. A. Bonn, W. N. Hardy, R. Liang, and R. H. Heffner, Science **292**, 1692 (2001).

[55] J. Xia, E. Schemm, G. Deutscher, S. A. Kivelson, D. A. Bonn, W. N. Hardy, R. Liang, W. Siemons, G. Koster, M. M. Fejer, and A. Kapitulnik, Phys. Rev. Lett. **100**, 127002 (2008).

[56] S. A. Kivelson, I. P. Bindloss, E. Fradkin, V. Oganesyan, J. M. Tranquada, A. Kapitulnik, and C. Howald, Rev. Mod. Phys. **75**, 1201 (2003).

[57] C. M. Varma, Phys. Rev. B **55**, 14554 (1997); Phys. Rev. Lett. **83**, 3538 (1999).

[58] S. Chakravarty, R. B. Laughlin, D. K. Morr, and C. Nayak, Phys. Rev. B **63**, 094503 (2001).